of MLCT transitions with different properties (e.g., one of them is sensitive to solvent polarity, and the other one is practically insensitive) in the same complex.

The asymmetry in the bridging ligands induced by the different metal fragments affects some properties of the electronic transitions related to the dpp ligands (e.g., extinction coefficients of the LC bands).

The different geometry of the bridges appears to be a key factor for the communication between the metal moieties in the dinuclear complexes. Intramolecular energy transfer from the photoreactive Ru fragment containing carbonyls to the $Ru(\eta^6\text{-}C_6H_6)Cl$ fragment is apparently an effective deactivation process for the 2,5-dpp complex, whereas this is not the case for the 2,3-dpp isomer. As a consequence, complex **5** maintains a strong photoreactivity in solution, typical of ruthenium(II) polypyridine carbonyl complexes, whereas complex **6** exhibits a 20 times lower photoreactivity.

Acknowledgment. We wish to thank Prof. V. Balzani for helpful discussions. This work was supported by the CNR and by the Ministero della Pubblica Istruzione.

Contribution from the Department of Chemistry, Northern Illinois University, DeKalb, Illinois 60115

Magnetic Circular Dichroism Spectra for the $Au_9(PPh_3)_8^{3+}$ Ion

Huey-Rong C. Jaw and W. Roy Mason*

Received June 19, 1990

Electronic absorption and magnetic circular dichroism (MCD) spectra in the vis-UV range 1.66–3.60 μm^{-1} are reported for $[Au_9(PPh_3)_8]X_3$ ($X = NO_3^-, ClO_4^-$) salts in acetonitrile solution at room temperature. The MCD spectra consist of *B* terms, are generally better resolved, and show more distinct spectroscopic features than the absorption spectra. The spectra are interpreted in terms of D_{2h} skeletal geometry and MO's that are approximated by 6s orbitals on the Au atoms. The lowest energy excited configurations and states are assumed to be σ framework localized. MCD *B* term signs are determined from two-centered σ-orbital overlaps within the cluster complex ion.

Introduction

An interesting aspect of gold chemistry is the formation of homonuclear cluster complexes by gold in low valence states (between 0 and 1).[1] The best characterized examples are complexes that range in nuclearity from Au_4 to Au_{13} and contain tertiary phosphine ligands. These cluster complexes are unique in that they are held together by unsupported Au–Au interactions and feature centered and noncentered structures. The nature of the electronic structure and the Au–Au bonding in these complexes has been the subject of several studies ranging from simple Hückel MO schemes to more elaborate Dirac scattered-wave calculations that include relativistic effects.[2-5] However, there has been a notable lack of experimental corroboration for these electronic structural models. There have been some electronic spectra reported for several cluster complexes both from solution measurements and from diffuse reflectance on solid compounds,[1,4a] but these spectra have not yet been interpreted in detail. The lack of interpretation may be partly due to the large number of possible excited states that can be visualized as the nuclearity of the complex increases. This situation is unfortunate because electronic spectroscopic data have value in providing an experimental basis for electronic structure and in providing information about low-energy excited states and the empty MO's of the complex under study. In order to address this problem of spectral interpretation, we have undertaken a study of the electronic absorption spectra of representative gold cluster complexes aided by magnetic circular dichroism (MCD) spectra. In this paper the absorption and MCD spectra for the $Au_9(PPh_3)_8^{3+}$ ion in acetonitrile solution are reported and are interpreted within an MO framework that is limited to σ cluster framework orbitals.

Experimental Section

Octakis(triphenylphosphine)enneagold trinitrate, $[Au_9(PPh_3)_8](NO_3)_3$, was prepared from $Au(PPh_3)(NO_3)$[6] by reduction with $NaBH_4$ in ethanol solution according to the literature method.[7] The dark green solid, which was recrystallized from CH_3CN, gave satisfactory elemental analysis and had a UV–vis spectrum in ethanol that compared favorably with the published spectrum.[1,4a] The perchlorate salt was prepared by dissolving the nitrate salt in ethanol and adding a concentrated solution of $LiClO_4$.[7] The green precipitate gave satisfactory analysis for $[Au_9(PPh_3)_8](ClO_4)_3$. *Caution: potential perchlorate hazard!*

Absorption spectra were measured for acetonitrile solutions by means of a Cary 1501 spectrophotometer. Absorption and MCD spectra were recorded simultaneously and synchronously along the same light path by means of a spectrometer described previously.[8] A magnetic field of 7.0 T was obtained from a superconducting magnet system (Oxford Instruments SM2-7, fitted with a room-temperature bore tube). Spectral grade acetonitrile was used throughout, and all spectra were corrected for solvent blank. Because of the strong absorption due to the phenyl substituents and, in the case of the nitrate salt, the nitrate ion, spectral measurements were limited to energies below 3.6 μm^{-1}. Below this energy the ClO_4^- and NO_3^- salts gave virtually identical absorption and MCD spectra and obeyed Beer's law to within experimental error in the concentration range 10^{-4}–10^{-5} M. The solutions neither were light sensitive nor exhibited any changes during the time required to make the spectral measurements (typically 1.5 h).

Table I. Spectral data for $[Au_9(PPh_3)_8](NO_3)_3$ in Acetonitrile

	absorption			MCD	
band no.	$\bar{\nu}$, μm^{-1}	λ, nm	ϵ, M^{-1} cm^{-1}	$\bar{\nu}$, μm^{-1}	$\Delta\epsilon_M$, $(M\ cm\ T)^{-1}$
				1.83	−0.12
				2.10	+0.91
I	2.26	443	16 200	2.21	+0.62[a]
				2.37	−0.76[a]
II	2.64	379	26 000[a]	2.60	−4.17
III	2.90	345	39 000[a]	2.86	−0.93
IV	3.19	314	62 000	3.25	−7.84
				3.40	−3.84[a]

[a] Shoulder.

Results and Discussion

The electronic absorption and MCD spectra for $[Au_9(PPh_3)_8](NO_3)_3$ in acetonitrile solution at room temperature are presented in Figure 1, while quantitative spectral data are collected in Table I. The MCD spectrum is generally better resolved and reveals more features than the absorption spectrum. For example,

(1) For a general review of gold clusters see: Hall, K. P.; Mingos, D. M. P. *Prog. Inorg. Chem.* **1984**, *32*, 237.
(2) Mingos, D. M. P. *J. Chem. Soc., Dalton Trans.* **1976**, 1163.
(3) van der Velden, J. W. A.; Stadnik, Z. M. *Inorg. Chem.* **1984**, *23*, 2640.
(4) (a) Mingos, D. M. P. *Polyhedron* **1984**, *3*, 1289. (b) Mingos, D. M. P.; Slee, T.; Zhenyang, L. *Chem. Rev.* **1990**, *90*, 383.
(5) (a) Arratia-Perez, R.; Ramos, A. F.; Malli, G. L. *Phys. Rev. B* **1989**, *39*, 3005. (b) Ramos, A. F.; Arratia-Perez, R.; Malli, G. L. *Phys. Rev. B* **1987**, *35*, 3790. (c) Arratia-Perez, R.; Malli, G. L. *J. Chem. Phys.* **1986**, *84*, 5891. (d) Arratia-Perez, R.; Malli, G. L. *Chem. Phys. Lett.* **1986**, *125*, 143.
(6) Nichols, D. I.; Charleston, A. S. *J. Chem. Soc. A* **1969**, 2581.
(7) Cariati, F.; Naldini, L. *J. Chem. Soc., Dalton Trans.* **1972**, 2286.
(8) Mason, W. R. *Anal. Chem.* **1982**, *54*, 646.

0020-1669/91/1330-0275$02.50/0

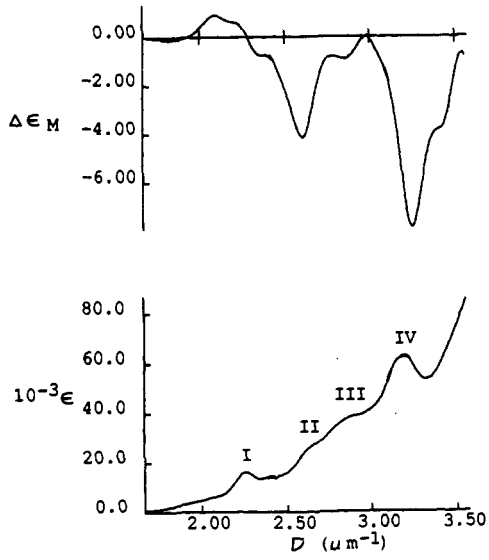

Figure 1. Electronic absorption (lower curve) and MCD (upper curve) spectra for $[Au_9(PPh_3)_8](NO_3)_3$ in CH_3CN at room temperature. $\Delta\epsilon_M$ has units of $(M\ cm\ T)^{-1}$.

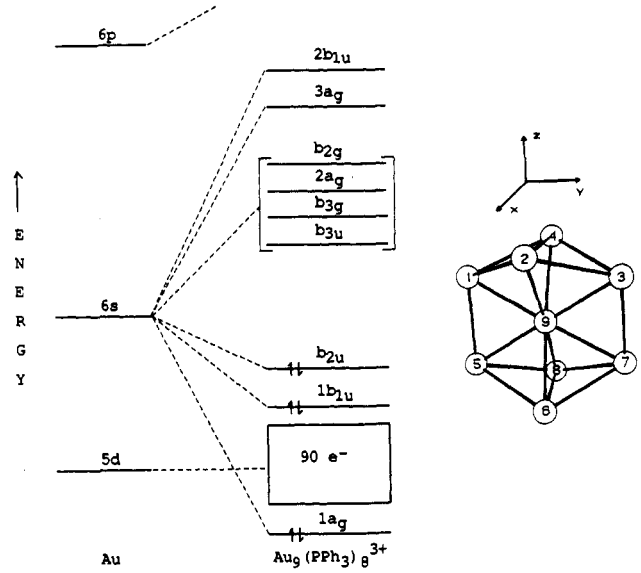

Figure 2. Molecular orbital energy levels for $Au_9(PPh_3)_8^{3+}$ assuming D_{2h} symmetry and primarily Au 6s framework bonding. The atom labeling and coordinate system are indicated to the right.

there are two MCD features at 1.8 μm^{-1} (weak negative minimum) and 2.1 μm^{-1} (positive maximum), which correspond to the broad unresolved tail on the low-energy side of band I. The MCD spectrum thus demonstrates the presence of transitions to at least two excited states lower in energy than the state associated with band I. Similarly, negative MCD features at 2.37 and 3.40 μm^{-1} have no resolved counterparts in the absorption spectrum but reveal the presence of weak transitions obscured by the stronger bands in the absorption spectrum. The bands labeled I–IV in the absorption spectrum all have high molar absorptivity ($\epsilon \sim 16200$–$62000\ M^{-1}\ cm^{-1}$; Table I) and are logically ascribed to allowed electronic transitions. These bands are unlikely to be due to the ligand phenyl absorptions because acetonitrile spectra for free PPh_3 and coordinated PPh_3 in a typical Au(I) complex $(Au(PPh_3)Cl)$ exhibit the lowest energy phenyl absorptions at energies above 3.5 μm^{-1}. Also the similarity of the spectra for the NO_3^- and ClO_4^- salts (Experimental Section) shows that the NO_3^- absorptions do not interfere in the region below 3.6 μm^{-1}. The spectra presented in Figure 1 are therefore reasonably attributed to intramolecular transitions of the $Au_9(PPh_3)_8^{3+}$ cluster framework. In order to further describe the nature of these transitions, the cluster structure must be taken into account. This is by no means a trivial matter because the solution structure of the $Au_9(PPh_3)_8^{3+}$ ion is not known.

Molecular Structure of the $Au_9(PPh_3)_8^{3+}$ Ion. Gold cluster complexes of the type $[Au_9(PAr_3)_8]X_3$ are known to exhibit two different polyhedral skeletal structures in the solid state, depending upon the arylphosphine and the counterion X.[1] Indeed for Ar = *p*-C_6H_4OMe and X = NO_3^- the two different skeletal isomers were both crystallized and structurally characterized:[9] (1) a green tetragonal modification that contains a cation with D_{2h} skeletal symmetry derived from a centered icosahedron, **1**, and (2) a golden brown orthorhombic modification that contains a centered crown cation of D_{4d} local but C_{2v} crystallographic symmetry, **2**. The

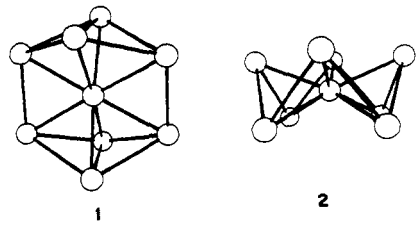

1

2

observation of these two different modifications of the same salt has prompted the suggestion that the potential surface interconnecting the two alternative skeletal structures is reasonably "soft".[1,4a] Furthermore, the electronic spectra from diffuse reflectance on solid salts containing cations with the different skeletal structures **1** or **2** are different,[1] but when these salts are dissolved, the solution spectra are identical.[9] This observation has prompted the suggestion of a common solution structure.[9] Solution NMR spectra for the $Au_9(PAr_3)_8^{3+}$ cluster cations reveal only single proton-decoupled ^{31}P resonances, which show no broadening at low temperature (to −90 °C).[9,10] This behavior suggests stereochemical nonrigidity on the NMR time scale.[4a] Therefore, while the green $[Au_9(PPh_3)_8]X_3$ (X = NO_3^-, ClO_4^-) salts investigated here can be reasonably inferred to contain cations with skeletal structure **1** based on diffuse reflectance,[1] the solution structure of the cluster cation remains unknown and is probably nonrigid. In order to analyze the absorption and MCD spectra and present an interpretation, an assumption is arbitrarily made that the solution structure of the $Au_9(PPh_3)_8^{3+}$ cation is similar to **1** (D_{2h} skeletal symmetry). In view of the solid structures, the solution structure is unlikely to be very different from either **1** or **2** and, in addition, conclusions based upon the assumption of **1** will not be very different from analogous conclusions based on **2**.

Electronic Excited States and MCD Terms. An earlier Hückel MO treatment of D_{2h} Au_9^{3+} clusters began with the assumption that the skeletal bonding involved primarily σ interaction among Au 6s orbitals.[2] The filled 5d orbitals were considered to be "corelike", and the empty 6p orbitals were assumed to be too high in energy to participate strongly in bonding. The MO scheme was elaborated upon more recently by some extended Hückel MO calculations,[3] but the essential features were retained. The energy level scheme is shown in Figure 2,[11] and the one-electron MO's are given in Table II. The diamagnetic ground-state electron configuration is assumed to be $...(1b_{1u})^2(b_{2u})^2$ and is designated ^1A_g. Electric dipole allowed transitions are permitted to B_{1u}(*z*-polarized), B_{2u}(*y*-polarized), and B_{3u}(*x*-polarized) excited states. Because of strong Au spin–orbit coupling, singlet and triplet excited states will become intermixed and transitions to formally spin-forbidden triplet states can gain considerable intensity. The lowest energy excited configurations are collected in Table III.

(9) Briant, C. E.; Hall, K. P.; Mingos, D. M. P. *J. Chem. Soc., Chem. Commun.* **1984**, 290.

(10) Vollenbroek, F. A.; van den Berg, J. P.; van der Velden, J. W. A.; Bour, J. J. *Inorg. Chem.* **1980**, *19*, 2685.

(11) The symmetry labels in Figure 2 differ slightly from those in ref 2 because of a difference in coordinate system: b_{3u} (*x*) and b_{2u} (*y*) have been interchanged. The coordinate system and atom labeling used here are shown in Figure 2.

Table II. One-Electron Molecular Orbitals

symmetry	energy[a]	MO wave function[b]
$1a_g$	$2\sqrt{2}\beta_1 + (3/2)\beta_2$	$(1/4)(\phi_1 + \phi_2 + \phi_3 + \phi_4 + \phi_5 + \phi_6 + \phi_7 + \phi_8 + 4\sqrt{2}\phi_9)$
$1b_{1u}$	$2\beta_2$	$(1/2\sqrt{2})(\phi_1 + \phi_2 + \phi_3 + \phi_4 - \phi_5 - \phi_6 - \phi_7 - \phi_8)$
b_{2u}	β_2	$(1/2)(\phi_1 - \phi_3 + \phi_5 - \phi_7)$
b_{3u}	$-\beta_2$	$(1/2)(\phi_2 - \phi_4 + \phi_6 - \phi_8)$
b_{3g}	$-\beta_2$	$(1/2)(\phi_1 - \phi_3 - \phi_5 + \phi_7)$
$2a_g$	$-\beta_2$	$(1/2\sqrt{2})(\phi_1 - \phi_2 + \phi_3 - \phi_4 + \phi_5 - \phi_6 + \phi_7 - \phi_8)$
b_{2g}	$-\beta_2$	$(1/2)(\phi_2 - \phi_4 - \phi_6 + \phi_8)$
$3a_g$	$2\sqrt{2}\beta_1 + (3/2)\beta_2$	$(1/4)(\phi_1 + \phi_2 + \phi_3 + \phi_4 + \phi_5 + \phi_6 + \phi_7 + \phi_8 - 4\sqrt{2}\phi_9)$
$2b_{1u}$	$-2\beta_2$	$(1/2\sqrt{2})(\phi_1 - \phi_2 + \phi_3 - \phi_4 - \phi_5 + \phi_6 - \phi_7 + \phi_8)$

[a] Hückel MO exchange integrals: β_1 from radial overlap of ϕ_9 with $\phi_1, \phi_2, \ldots, \phi_8$; β_2 from adjacent tangential overlap of ϕ_1 with ϕ_2, ϕ_1 with ϕ_5, etc. The atom labeling and coordinate system are as in Figure 2. [b] ϕ_i = Au 6s orbital on atom i.

Table III. Excited Configurations and States

excited confgn[a]	zero-order states	spin–orbit states[b]
$(b_{2u})(b_{3g})$	$^1B_{1u}$	$1B_{1u}$
	$^3B_{1u}$	(A_u), $1B_{2u}$, $1B_{3u}$
$(b_{2u})(2a_g)$	$^1B_{2u}$	$2B_{2u}$
	$^3B_{2u}$	$2B_{3u}$, (A_u), $2B_{1u}$
$(b_{2u})(b_{2g})$	^1A_u	(A_u)
	^3A_u	$3B_{1u}$, $3B_{2u}$, $3B_{3u}$
$(1b_{1u})(b_{3g})$	$^1B_{2u}$	$4B_{2u}$
	$^3B_{2u}$	$4B_{3u}$, (A_u), $4B_{1u}$
$(1b_{1u})(2a_g)$	$^1B_{1u}$	$5B_{1u}$
	$^3B_{1u}$	(A_u), $5B_{2u}$, $5B_{3u}$
$(1b_{1u})(b_{2g})$	$^1B_{3u}$	$6B_{3u}$
	$^3B_{3u}$	$6B_{2u}$, $6B_{1u}$, (A_u)

[a] Filled orbitals omitted. Ground-state configuration = ... $(1b_{1u})^2(b_{2u})^2$, ^1A_g. [b] Electric dipole forbidden A_u states in parentheses.

Table III also lists the zero-order singlet and triplet excited states in the absence of strong spin–orbit interaction and the spin–orbit states in the presence of strong interaction. These latter states, characterized by lack of spin multiplicity superscripts, provide the basis for spectral interpretation.

The MCD spectra for $Au_9(PPh_3)_8^{3+}$ can exhibit only B terms[12] because the D_{2h} symmetry has only 2-fold rotational symmetry and therefore no true degeneracies. The absence of degenerate ground and excited states excludes MCD A terms; the diamagnetic ground state requires C terms be absent also.[12] The MCD B terms arise from the magnetic field induced mixing of the B_{1u}, B_{2u}, and B_{3u} states and is given in terms of the $\bar{B}_0$ parameter for the space-averaged case appropriate for anisotropic molecules in solution by eq 1.[12] In eq 1 the $\bar{B}_0$ parameter for the transition $^1A_g \rightarrow B_{\alpha u}(J)$, α = 1, 2, or 3 at energy W_J, is given by a sum of contributions from the states $B_{\beta u}(K)$ at energies W_K; μ_B = Bohr magneton; $\Delta W_{KJ} = W_K - W_J$, the energy difference between the states K and J; $\mu = -\mu_B(L + 2S)$ and $\mathbf{m} = e\mathbf{r}$, the magnetic and electric moment operators, respectively. The calculation of B terms is difficult unless the summation of the states K in eq 1 can be reduced to only a few terms. This is often possible because the inverse dependence on ΔW_{KJ} makes the largest contributions from states closest in energy. Furthermore, since the $B_{\alpha u}$ states are defined in terms of antisymmetrized one-electron MO's, interactions are restricted for reasons of orthogonality to those states that differ by only one spin orbital. The metal-localized MO's are approximated by Au atomic orbitals, and in the present analysis the ϕ_i were initially assumed to be Au 6s orbitals (Table II). The magnetic moment reduced matrix elements (RME's) of eq 1 are therefore due entirely to two-centered contributions because a 6s orbital on a single center has no angular momentum and therefore no magnetic moment. The two-centered orbital angular momentum terms necessary to evaluate the magnetic moment RME's were approximated by the relation[13]

$$\bar{B}_0(B_{\alpha u}(J),B_{\beta u}(K)) = -\frac{4}{3\mu_B}\,\mathrm{Re}\left[\sum_{\substack{K\neq J\\ \alpha\neq\beta}} \frac{\langle B_{\alpha u}(J)||\mu^{b}{}_{r\pi}||B_{\beta u}(K)\rangle}{\Delta W_{KJ}} \times \langle {}^1A_g||\mathbf{m}^{b}{}_{\alpha u}||B_{\alpha u}(J)\rangle\langle B_{\beta u}(K)||\mathbf{m}^{b}{}_{\beta u}||{}^1A_g\rangle\right] \quad (1)$$

$$\langle \phi_a|l_\alpha|\phi_b\rangle \cong -iT_{ab}(\beta_{a\gamma b} - \gamma_{a\beta b})$$

where T_{ab} is an overlap integral between ϕ_a and ϕ_b (assumed to be positive for positive phases for ϕ_a and ϕ_b) and α, β, and γ are Cartesian coordinates of atom a or b referred to the center of the coordinate system. The approach taken here is to attempt to predict the *sign* of the $\bar{B}_0$ contributions by using eq 1, together with the approximations indicated above; quantitative calculations of $\bar{B}_0$ magnitudes were not attempted because they cannot be very precise in view of the complexity of the problem and the approximations involved. The treatment of B terms was initially carried out only for the states of predominantly singlet origin, which are expected to give the strongest bands in the spectra. The calculation of $\bar{B}_0$ for transitions to $B_{\alpha u}$ states of triplet parentage requires a further layer of approximation from estimation of the singlet character resulting from the spin–orbit interaction. Table IV summarizes the $\bar{B}_0$ contributions from interactions among the predominantly singlet states of the excited configurations of Table III: $1B_{1u}$, $2B_{2u}$, $4B_{2u}$, $5B_{1u}$, and $6B_{3u}$; $A_u(^1A_u)$ was not considered because transitions to this state are orbitally forbidden and therefore would be very weak. The properties of the $\bar{B}_0$ parameter are such that $\bar{B}_0(B_{\beta u}(K),B_{\alpha u}(J)) = -\bar{B}_0(B_{\alpha u}(J),B_{\beta u}(K))$ for a single pairwise interaction between states J and K.[12] Finally, it may be remarked that the *sign* determination of the $\bar{B}_0$ contributions is quite general for σ Au–Au interactions and will not likely be affected by the extent of hybridization of the Au atomic orbitals, provided the energy ordering is not changed. Thus, the assumption that ϕ_i = Au 6s can be replaced by $\phi_i = \lambda 6s + (1 - \lambda^2)^{1/2}6p$, an Au 6s6p hybrid, without loss of the generality.

Table IV. Contributions to B Terms

$B_{\alpha u}$ state[a]			$B_{\alpha u}$ state[a]		
J	K	$\bar{B}_0$ contribn	J	K	$\bar{B}_0$ contribn
$2B_{2u}$	$1B_{1u}$	pos	$5B_{1u}$	$4B_{2u}$	~0
$2B_{2u}$	$5B_{1u}$	neg	$5B_{1u}$	$6B_{3u}$	~0
$1B_{1u}$	$4B_{2u}$	neg	$4B_{2u}$	$6B_{3u}$	neg

[a] State K is assumed to be higher in energy than state J, so that ΔW_{KJ} is positive.

Interpretation of the Absorption and MCD Spectra. On the basis of the MO scheme in Figure 2, together with the states of the low-energy excited configurations (Table III), bands I–IV in the absorption spectrum (Figure 1) are assigned as transitions to the predominantly singlet spin–orbit states $2B_{2u}$, $1B_{1u}$, $5B_{1u}$, and $4B_{2u}$, respectively. The transition to $6B_{3u}$ is assumed to be higher in energy than band IV and obscured by the rising absorption $\geq$3.3 μm^{-1}. The shoulder in the MCD spectrum at 3.4 μm^{-1} may signal this transition. Some support for these assignments of the absorption spectrum can be obtained from an interpretation of the B term pattern observed in the MCD spectrum. Unfortunately, a full and complete explanation of the MCD spectrum cannot be given because high-energy transitions beyond our measurement capability will exert a significant influence on the shape of the observed MCD bands, especially for bands III and IV. Rationalization of B term signs can be given with greater confidence for

(12) Piepho, S. B.; Schatz, P. N. *Group Theory in Spectroscopy with Applications to Magnetic Circular Dichroism*; Wiley-Interscience: New York, 1983. This reference describes the standard (Stephens) definitions and conventions that are used here.

(13) VanCott, T. C.; Rose, J. L.; Misener, G. C.; Williamson, B. E.; Schrimpf, A. E.; Boyle, M. E.; Schatz, P. N. *J. Phys. Chem.* **1989**, *93*, 2999.

bands I and II, however, because the states associated with these lower energy bands are farther removed in energy (large ΔW in eq 1) from the high-energy transitions. The ordering of excited states implied from the assignment of bands I–IV indicates the largest contribution to the B term for the transition to $2B_{2u}$ will be from the $1B_{1u}$ state and will be positive (Table IV). A smaller negative contribution from the $5B_{1u}$ state, which is farther removed and higher in energy, is interpreted as being insufficient to alter the sign imposed by the $1B_{1u}$ contribution. The observed MCD for band I shows a positive, though somewhat weak, B term and is thus consistent with a larger positive $\bar{B}_0$ contribution and a smaller negative $\bar{B}_0$ contribution. In contrast to the MCD spectrum for band I, the $\bar{B}_0$ contributions for the transition to $1B_{1u}$ assigned to band II are negative from $2B_{2u}$ at lower energy and negative from $4B_{2u}$ at higher energy. The two negative contributions thus reinforce each other, giving a larger negative B term consistent with experiment. The shoulder band III assigned to the transition to $5B_{1u}$ is predicted to have a positive $\bar{B}_0$ contribution from the lower energy $2B_{2u}$ state and negligible contributions from the other states of Table III. The observed MCD spectrum shows a weaker negative feature at 2.86 μm^{-1}. It is reasonable to assume that other high-energy states beyond our measurements make negative contributions that are slightly larger than the positive $\bar{B}_0$ contribution from $2B_{2u}$. The observed MCD is certainly "more positive" than for band II, but it is still negative. Finally the transition to the $4B_{2u}$ state, band IV, is expected to have a strong negative $\bar{B}_0$ contribution from the higher energy $6B_{3u}$ state, but the very strong negative MCD must also signal substantial negative contributions from the higher energy states. As noted above, the B term interpretation for bands III and IV are subject to the uncertainties of the contributions from the higher energy states, which are beyond our measurement capabilities; the absorption due to the PPh_3 ligands and to the NO_3^- ion will likely preclude a detailed consideration of these states, even if spectra were extended to higher energy.

The MCD features at 1.83, 2.10, and 2.37 μm^{-1}, which indicate weak transitions unresolved in the absorption, are logically assigned to transitions to spin–orbit states of predominantly triplet parentage. The position of the 1.83- and 2.10-μm^{-1} features to energy lower than that of band I suggests assignments to $2B_{3u}$ and $2B_{1u}$, respectively, and the 2.37-μm^{-1} MCD band on the red side of the stronger MCD associated with band II may be due to $1B_{3u}$ or $1B_{2u}$. In each case, the MCD bands are 0.11–0.4 μm^{-1} below the bands associated with the corresponding states of singlet origin. The singlet–triplet energy separation is similar to, but somewhat smaller than, that observed for mononuclear and binuclear Au(I) complexes (typically 0.3–0.6 μm^{-1})[14] and therefore seems reasonable in view of the lower average metal oxidation state in $Au_9(PPh_3)_8^{3+}$ ($+^1/_3$ per Au). A limited effort was made to determine the B term signs for the transitions to these predominantly triplet states, but as explained above, the additional approximations from the spin–orbit interaction that are necessary introduce uncertainties. On the assumptions that the magnetic interaction between $2B_{3u}$ and $2B_{1u}$ dominates the sign of the $\bar{B}_0$ for $2B_{3u}$ and that the singlet character for this state arises only from the high-energy $6B_{3u}$ state (the only B_{3u} state of singlet origin), eq 1 predicts a weak negative B term for $2B_{3u}$ consistent with the weak negative MCD at 1.83 μm^{-1}. The B term for $2B_{1u}$ derives its intensity from the $1B_{1u}$ and $5B_{1u}$ states, which are closer in energy. Therefore the larger B term for $2B_{1u}$ at 2.10 μm^{-1} is reasonable. The sign of the B term could not be predicted with confidence however because of the numerous contributions of different magnitudes involved. The B term at 2.37 μm^{-1} is assigned to the transition to the $1B_{2u}$ state from intensity arguments. The transition to the alternative $1B_{3u}$ is expected to be weak because of a low singlet character from the high-energy $6B_{3u}$.

Concluding Remarks. It is encouraging that the simple MO scheme of Figure 1 based on σ Au–Au interaction primarily from 6s orbitals[2] is capable of providing a satisfactory interpretation of the absorption and MCD spectra for $Au_9(PPh_3)_8^{3+}$. Of course, there may be other possible schemes that can explain the spectra, but the MCD B term signs of the lowest energy states narrow the acceptable possibilities. For example, a limited investigation of 6p orbital Au–Au interaction was performed for the skeletal bonding. This case may be viewed as a logical extension of the Au–Au interaction in binuclear digold(I) complexes containing diphosphine ligands, where the lowest energy empty MO's are believed to be 6p orbital based.[14b] Such low-lying 6p orbitals can be viewed as a consequence of strong σ-donor phosphine ligand bonding to the Au 6s orbital, which would destabilize 6s-based MO's to energies *higher* than those of the 6p's. The lowest energy excited configuration for $Au_9(PPh_3)_8^{3+}$ on the assumption of a 6p-based scheme is expected to result from $6p\sigma \rightarrow 6p\pi$ excitations. The $\bar{B}_0$ contributions from eq 1 for the lowest energy allowed states were determined from one-centered $6p\pi$ MO's to be negative, and the $\sigma \rightarrow \pi$ electric moments for transitions to these states were very small. Thus the 6p-based σ and π interactions to a first approximation do not fit the experimental observation of a positive B term for band I. A lower involvement of the 6s orbital in Au–PPh_3 bonding, and therefore greater Au–Au 6s bonding, might be anticipated from the lower metal charge in the $Au_9(PPh_3)_8^{3+}$ cluster complex compared to that in typical Au(I) complexes. Furthermore, the relativistic properties[15] of the Au 6s orbital (greater stability and radial contraction) favor 6s–6s Au–Au bonding interaction over analogous 6p–6p interaction. In the latter case, strong spin–orbit coupling (another relativistic effect) lowers the energy of $6p_{1/2}$, but the $6p_{1/2}$–$6p_{1/2}$ interaction is not favorable for bonding because σ-bonding overlap is counterbalanced by a nearly equal π-antibonding overlap of the Dirac spin orbitals.[16]

Acknowledgment is made to the donors of the Petroleum Research Fund, administered by the American Chemical Society, for support of this work.

(14) (a) Savas, M. M.; Mason, W. R. *Inorg. Chem.* **1987**, *26*, 301. (b) Jaw, H.-R. C.; Savas, M. M.; Rogers, R. R.; Mason, W. R. *Inorg. Chem.* **1989**, *28*, 1028. (c) Jaw, H.-R. C.; Savas, M. M.; Mason, W. R. *Inorg. Chem.* **1989**, *28*, 4366.

(15) Pyykkö, P. *Chem. Rev.* **1989**, *88*, 563 and references therein.

(16) Pitzer, K. S. *Acc. Chem. Res.* **1979**, *12*, 271; *J. Chem. Phys.* **1975**, *63*, 1032.